Comparison of Tumor Non-specific and PD-L1 Specific Imaging by Near-Infrared Fluorescence/Cerenkov Luminescence Dual-Modality In-situ Imaging

Linhan Zhang, MD[1],*, Lianmeng Zhao, MS[2],*, Xue Lin, MD[3],
Sheng Zhao, MD[3], Wenbin Pan, MS[3], Dandan Wang, MD[3],
Zhongqi Sun, MD[3], Jinping Li, MD[3], Zonghui Liang, MD[4],
Rongjun Zhang, MS[5] and Huijie Jiang, MD[3] iD

Abstract

Background: Labeled antibodies are excellent imaging agents in oncology to non-invasively visualize cancer-related antigens expression levels. However, tumor tracer uptake (TTU) of specific antibodies in-vivo may be inferior to non-specific IgG in some cases.
Objectives: To explore factors affecting labeled antibody visualization by PD-L1 specific and non-specific imaging of nude mouse tumors.
Methods: TTU was observed in RKO model on Cerenkov luminescence (CL) and near-infrared fluorescence (NIRF) imaging of radionuclide ^{131}I or NIRF dyes labeled Atezolizumab and IgG. A mixture of NIRF dyes labeled Atezolizumab and ^{131}I-labeled IgG was injected, and TTU was observed in the RKO and HCT8 model by NIRF/CL dual-modality in-situ imaging. TTU were observed by ^{131}I-labeled Atezolizumab and IgG in-vitro distribution.
Results: Labeled IgG concentrated more in tumors than Atezolizumab. NIRF/CL imaging in 24 to 168 h showed that TTU gradually decreased over time, which decreased more slowly on CL imaging compared to NIRF imaging. The distribution data in-vitro showed that TTU of ^{131}I-labeled IgG was higher than that of ^{131}I-labeled Atezolizumab at any time point.
Conclusion: Non-specific IgG may not be suitable as a control for Atezolizumab in comparing tumor PD-L1 expression in nude mice via labeled antibody optical imaging under certain circumstances.

[1]Department of Nuclear Medicine, The First Affiliated Hospital of Harbin Medical University, Harbin, China
[2]Ultrasound Department, Heilongjiang Provincial Hospital, Harbin, China
[3]Department of Radiology, The Second Affiliated Hospital of Harbin Medical University, Harbin, China
[4]Department of Radiology, Jing'an District Centre Hospital (Jing'an Branch of Huashan Hospital), Shanghai, China
[5]Jiangsu Institute of Nuclear Medicine, Wuxi, China

*Both authors are co-first authors and contributed equally to this study.

Corresponding Authors:
Zonghui Liang, Department of Radiology, Jing'an District Centre Hospital (jing'an Branch of Huashan Hospital), Shanghai 200040, China.
Email: liang_zh@fudan.edu.cn

Rongjun Zhang, Jiangsu Institute of Nuclear Medicine, Wuxi 214063, China.
Email: zhangrongjun@jsinm.org

Huijie Jiang, The Second Affiliated Hospital of Harbin Medical University, Harbin 150086, China.
Email: jianghuijie@hrbmu.edu.cn

Introduction

Programmed cell death-Ligand 1 (PD-L1) expression in tumor cells is a potential biomarker for predicting anti-programmed cell death-1/PD-L1 (anti-PD-1/PD-L1) immunotherapeutic responses.[1] Molecular imaging can overcome many drawbacks of immunohistochemical testing,[2] and has become increasingly a useful tool for detecting PD-L1 expression in tumors.[3-6] Atezolizumab (MPDL3280A), as a monoclonal antibody IgG1 anti-PD-L1, has been approved by the U.S. Food and Drug Administration (FDA) as a single drug or combined with other chemotherapeutic drugs for various tumor diseases.[7-9] A number of studies have shown that molecular imaging of Atezolizumab labeled with radionuclides or fluorescent dyes enables accurate detection of PD-L1 expression levels in different tumors.[10-14] Our team found a correlation between tumor cell PD-L1 expression levels and radionuclide ^{131}I-labeled Atezolizumab (^{131}I-Atezolizumab) in previous in-vivo and in-vitro studies,[15] and also observed that ^{131}I-Atezolizumab (37 MBq, 24.4 µg protein) remained in human-derived tumors with high PD-L1 expression for a long time and inhibited tumor growth, while no significant weight loss occurred in mice.[16] This may be the result of radioimmunotherapy. Therefore, we conducted a study on radioimmunotherapy for the PD-L1 target, which was based on the ^{131}I-Atezolizumab as the therapeutic agent and the ^{131}I-labeled human non-specific IgG1 (^{131}I-IgG) as the isotype control in a human-derived tumor nude mouse model. After 11 days of treatment, we found that the tumor was significantly controlled in the ^{131}I-IgG treatment group and the tumor volume was even lower than in the ^{131}I-Atezolizumab treatment group. The results of Cerenkov luminescence imaging (CLI) in 11 days after injection of ^{131}I-IgG or ^{131}I-Atezolizumab were also consistent with the results of treatment. We were puzzled by the result. The biggest drawback is that optical imaging is a 2-dimensional image with limited surface penetration depth. Due to the heterogeneity of the tumor, the imaging results of slightly different body positions of the same mouse may be different. Dual-modality in-situ imaging overcomes the bias of results due to different body positions. So we injected a mixture of IRDye®800 CW labeled Atezolizumab (IR-Atezolizumab) and ^{131}I-IgG into the same mouse. Using different imaging methods of the 2 markers, non-specific and specific imaging of targeting PD-L1 were observed simultaneously on the same optical device.

Dual-modality in-situ imaging can obtain real-time information of 2 imaging methods, and may finally play the role of "1 + 1 > 2." The results achieved by PET/CT in the past 20 years are the most favorable proof. In addition, researchers working on dual-radionuclide PET/SPECT imaging avoided many wrong conclusions by dual-modality in-situ imaging, while reducing the number of animals needed to conclude by half.[17] Imaging of IRDye®800CW-labeled antibodies is mainly based on near-infrared fluorescence (NIRF) imaging that excites fluorescent dyes. Radionuclide ^{131}I CLI is the generation of high-energy band-point particles by ^{131}I beta decay, which produces an image of detectable light by Cerenkov radiation. Cerenkov light is mainly weighted towards the ultraviolet and blue part of the spectrum.[18] The 2 have different imaging modalities making NIRF/Cerenkov luminescence (NIRF/CL) dual-modality in-situ imaging possible. Some scholars had coupled IRDye®800 CW, radionuclide ^{89}Zr with monoclonal antibody for NIRF/CL in-situ imaging.[19,20] However, it is not reported that IRDye®800 CW and radionuclide were labeled with 2 different antibodies for NIRF/CL in-situ imaging. In this study, we performed homologous and heterologous controlled optical imaging of radionuclide ^{131}I or NIRF dyes labeled specific antibody Atezolizumab and non-specific antibody IgG in a human-derived tumor nude mouse model.

Methods

Cell Lines and Tumor Models

Human cancer cell lines including cervical cancer Hela, malignant melanoma A375, large cell lung cancer H460, colorectal cancer RKO and HCT8 were obtained from the Cell Bank of the Chinese Academy of Sciences. RKO cells were grown in MEM (Gibco, USA) medium. HCT8 and H460 cells were grown in RPMI 1640 (Biological Indus-tries, Israel) medium. Hela or A375 cells were cultured in DMEM (Gibco, USA) medium. All media were supplemented with 10% fetal bovine serum (FBS, Biological Indus-tries, Israel) and 1% penicillin streptomycin (Beyotime Biotechnology, China). All cells were cultured in 5% CO_2 incubator at 37 °C and the medium was changed once every 2 to 3 days. Cells in the logarithmic growth phase were used for cellular uptake analysis in-vitro and subcutaneous transplant tumor experiments in-vivo.

Female Balb/c nu mice aged 5-6 weeks were obtained from Changzhou Cavens Experimental Animal Co., Ltd and raised in SPF-level animal laboratories. After 1 week of adaptation, nude mice were injected with $(3-5) \times 10^6$ tumor cells under the armpits to establish RKO, HCT8, Hela, A375, and H460 human-derived tumor models. 0.5% sodium iodide solution was also drunk on and during imaging and treatment to seal thyroid tissue. All procedures were performed with the approval of the Institutional Animal Care and Use Committees of Jiangsu Institute of Nuclear Medicine.

Radiolabeling

Preparation of ^{131}I-IgG and ^{131}I-Atezolizumab. Following the method previously reported,[21] antibodies were labeled by Iodogen (1, 34,6-tetrachloro-3α,6α-diphenylglycoµril) method.

Briefly, 100 μl of phosphate buffer (PB, 0.25 mol/L, pH7.4) and 100 μg Atezolizumab (HY-P9904, MCE, USA) or human non-specific IgG1 (IgG, BE0297, BioXcell, USA) were added to the coating tube containing 50 μg Iodogen and mixed, and about 185 to 330 MBq Na^{131}I (Chengdu Gaotong Isotope Co., Ltd, China) was added and reacted 15 min after mixing at room temperature. 100 μl of PB (0.25 mol/L, pH 7.4) was added to terminate the reaction and left to stand for 10 min. Radiolabeled antibodies were purified by using a PD-10 columns (GE Healthcare, USA) with 20 mmol/L phosphate buffer saline (PBS) containing 0.2% bovine serum albumin (BSA) as the eluent. The radiochemical purity of the prepared ^{131}I-IgG or ^{131}I-Atezolizumab was determined by trichloroacetic acid precipitation. Radiochemical purity higher than 95% was used for experiments in-vivo.

Preparation of IR-Atezolizumab and IRDye®800 CW Labeled IgG (IR-IgG).

According to the instructions of IRDye® 800CW Protein Labeling Kit (LI-COR, USA), Atezolizumab or IgG was coupled with NIRF dyes. In short, 180 μl boric acid buffer (1.0 mol /L, pH8.6), 1.8 mg Atezolizumab or IgG and IR NHS (7.5 μl, 5 mg/ml) were mixed in turn and incubated at 25 °C for 2 h. The glycine solution (10 μl, 10 mg/mL) was added and reacted for 10 min, and 20 mmol/L PBS containing 0.2% BSA was used as the eluent to purify the labeled monoclonal antibody with PD-10 column. After the peak tubes were collected, the absorbance values at 260, 280, and 780 nm were measured by Nanodrop 2000 UV/VIS spectrophotometer, and the concentration of marker protein was determined.

Cellular Uptake

^{131}I-Atezolizumab and ^{131}I-IgG cell binding analysis was performed using Hela, A375, H460, RKO, and HCT8 cells. Each of cell suspensions (5×10^5 cells/tube, 100 μl, triplicate), RPMI1640 medium (100 μl) containing 10% FBS, and ^{131}I-Atezolizumab or^{131}I-IgG (100 μl, 2.79 ng, 3.7 kBq) were bathed at 37 °C for 1 h. To measure non-specific binding, non-radioactive Atezolizumab or IgG (100 μl, 558 ng) of 200-fold molar ratio were used instead of the above medium. After incubation, 700 μl of serum-containing medium cooled to 4 °C was added to each binding tube, and the supernatant was discarded by centrifugation, and each sample was counted in a gamma counter (Wizard 1480, Perkin-Elmer). The percent cellular uptake (% Cellular uptake) was expressed as the percentage of specific radioactivity retained in cells relative to the total radioactive tracer added.

^{131}I-IgG or ^{131}I-Atezolizumab was Used to Treat PD-L1 High Expression Tumor-Bearing Mice

Fifteen female nude mice were subcutaneously transplanted with PD-L1 high expression cells. After 6 days of transplantation, the tumor volume was about 60 to 100 mm^3. The mice were randomly divided into 3 groups: ^{131}I-IgG treatment group (33.3 MBq, 19 μg protein, n = 5), ^{131}I-Atezolizumab treatment group (33.3 MBq, 19 μg protein, n = 5) and untreated control group (n = 5). The technicians who did not know the grouping method were responsible for the measurement of tumor. The tumor was measured with vernier caliper every 2 to 3 days to record the tumor growth. The tumor volume was calculated by the following formula: tumor volume = (W)$^2 \times$ (Y) $\times$ 0.52. Y and W were larger and smaller vertical diameters respectively. The methods involved in the experiments were performed in accordance with the relevant guidelines and regulations for animal experiments. The trial could be terminated if at least one of the following criteria was met: tumor volume was greater than 1500 mm^3; overall weight decrease > 20%; tumor xenografts showed obvious ulcers, bleeding or abnormal behavior indicating pain or discomfort in animals.

HE Staining and Immunohistochemistry Analysis

On the 12th day after treatment, the tumor tissue was taken and immediately fixed with tissue fixative and embedded in paraffin. HE staining was passed through a serial process of dewaxing, dyeing, hydration, and drying. Immunohistochemical methods were used to detect the expression of Ki-67 in tumor tissues. After routine dewaxing and hydration of tissue slices, antigen was repaired with 10 mmol/L citrate buffer, endogenous peroxidase was blocked with 3% H$_2$O$_2$, and non-specific antigen was blocked with 3% BSA. The first antibody (ab16667, Abcam, UK) was added and incubated at 4 °C overnight. HRP labeled secondary antibody (Zhongshan Golden Bridge Biotechnology, China) was incubated at room temperature for 1 h. Sections were counterstained with haematoxylin, dehydrated, transparent and mounted with neutral balsam.

Small Animal NIRF Imaging

Six BALB/c mice transplanted with PD-L1 high expression cells were randomly divided into 2 groups of 3 mice each. IR-Atezolizumab and IR-IgG were injected respectively. The mice were kept in supine position under continuous anesthesia, and NIRF imaging (λex/em: 745/800 nm) was performed at different time points using IVIS Spectrum system (PerkinElmer, MA, USA).

^{131}I-IgG CLI in 5 Tumor Models

In order to evaluate the non-specific uptake of ^{131}I-IgG in different tumors, we conducted 2 studies on the subcutaneous xenograft models of 5 tumor cells. In the first study, cervical cancer Hela cells, melanoma A375 cells, large cell lung cancer H460 cells, colorectal cancer RKO, and HCT8 cells were transplanted subcutaneously into nude mice ($n = 3$/group). After 14 to 27 days of transplantation, all mice

were injected with ^{131}I-IgG (33.3 MBq, 19 μg protein) via tail vein. In the second study, HCT8 tumor model was re-established and ^{131}I-Atezolizumab (33.3 MBq, 19 μg protein) was injected for comparison with the first study. CLI (λex/em:closed/open) was performed on different tumor model mice at different time points (1-5 days) using an IVIS spectral imaging system. The mice were placed in the lateral recumbent position with continuous anesthesia. The average fluorescence intensity of the tumor and leg muscles was determined by Living Image® 4.5 software. Relative fluorescence intensity was determined by comparison of the two.

NIRF/CL Dual-Modality In-situ Imaging and Biodistribution Imaging

In order to eliminate the high fluorescence intensity caused by tumor growth stage, growth speed and individual differences of mice in non-specific imaging of mouse tumors, IR-Atezolizumab NIRF imaging and ^{131}I-IgG CL in-situ imaging were performed on PD-L1 high and low expression model (n = 4/group). In brief, the mixture (200 μl) of IR-Atezolizumab (70 μg protein), ^{131}I-IgG (33.3 Mbq, 17 μg protein), and IgG (53 μg protein) was injected into mice by tail vein. NIRF/CL dual-modality in-situ imaging was performed. For NIRF imaging (λex/em:745/800 nm) and CLI (λex/em: closed/open), the IVIS Spectrum Imaging System was used.

After 168 h of administration, all mice were euthanized for biodistribution imaging studies. Tumor and visceral tissues were obtained, which included heart, liver, spleen, lung, kidney, stomach (without contents), intestine (without contents), pancreas, leg muscles, mesenteric fat, thyroid, ovary, femur, brain, and blood. Tumor and visceral tissue samples were placed in a certain order on the surface dish, and NIRF/CL in-situ distribution imaging were performed. By using Living Image® 4.5 software, the contour of tissues, organs and tumors were manually delineated on white light channels, and the measurement parameters were adjusted to measure the average fluorescence intensity of tissues and organs at the same position and range in NIRF imaging and CLI. Relative fluorescence intensity was quantified by the ratio of average fluorescence intensity of each tissue to that of muscle.

[131]I-Atezolizumab and ^{131}I-IgG Biodistribution Studies in PD-L1 High Expression and Low Expression Model

Biodistribution experiments were performed as described previously.[15] In short, PD-L1 high and low expression tumor-bearing female mice were intravenously injected with ^{131}I-Atezolizumab or ^{131}I-IgG (1.2 MBq, 70 μg protein). Mice were euthanized at 24, 72, and 168 h after administration. (n = 4, 5/time point/group). The heart, liver, spleen, lung, kidney, stomach (without content), intestine

(without content), pancreas, leg muscle, mesenteric fat, thyroid, ovary, femur, brain, blood and tumor were collected, weighed and measured in a gamma counter. The percent injected dose per gram (%ID/g) was calculated by comparison to a weighed, diluted standard.

Statistics

The data met the normal distribution, expressed as mean ± standard deviation. Statistical analysis was performed using SPSS 11 software (SPSS Inc., USA). Two groups were compared using Student's T test. One-way ANOVA was used for comparison among multiple groups, and LSD-t test was used for pairwise comparison. $P < .05$ was considered significant.

Results

Binding to Cancer Cell Lines

Hela, A375, H460, RKO, and HCT8 cells did not bind to ^{131}I-IgG, but they were bound to ^{131}I-Atezolizumab to varying degrees. % Cellular uptake were (1.71 ± 0.48) %, (20.41 ± 1.17) %, (11.2 ± 0.72) %, (62.1 ± 1.56) %, and (2.35 ± 0.49) %, respectively (Figure 1).

Therapy Effect

Since RKO cells and ^{131}I-Atezolizumab had the highest binding capacity, we used the RKO xenotransplantation model to evaluate the radioimmunotherapy effect of ^{131}I-Atezolizumab on tumors. Figure 2a and b showed the changes of tumor volume and body weight with time after injection of ^{131}I-Atezolizumab or ^{131}I-IgG. On the 9th and 11th days in the ^{131}I-IgG treatment group, 2 mice showed significant weight loss, reaching 79.8% and 72.0% of their pre-treatment body weight, and were euthanized. After 11 days of treatment, the volumes of untreated group, ^{131}I-Atezolizumab treatment group, and ^{131}I-IgG treatment group were (510.8 ± 147.2) mm^3, (259.6 ± 114.3) mm^3, and (131.5 ± 74.3) mm^3, respectively. The tumor volumes of ^{131}I-Atezolizumab treatment group and ^{131}I-IgG treatment group were significantly smaller than that of the untreated group $(P = .007, .001)$. The tumor volume in the ^{131}I-IgG treatment group was lower than that in the ^{131}I-Atezolizumab treatment group, but the difference was not statistically significant $(P = .137)$. We were puzzled about this result, so we performed ^{131}I CLI on the surviving mice of the treatment group on 11 days of treatment. We found that ^{131}I-Atezolizumab treatment group had accumulation of radionuclides in the tumor, but the accumulation of radionuclides in ^{131}I-IgG treatment group was more obvious (Figure 2c), which was consistent with the results of tumor volume and body weight of mice. On the 12th day of treatment, all mice in the [131]I- IgG treatment group showed significant weight loss, which was 20% lower than
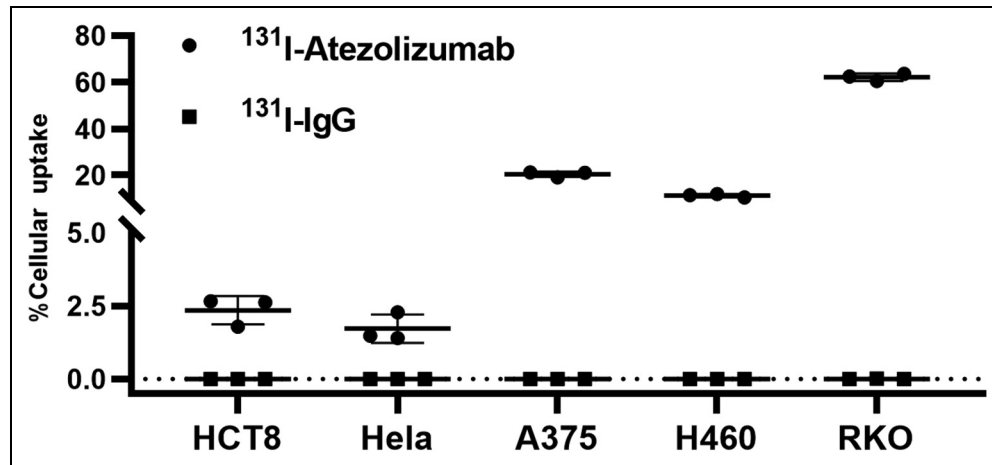
Figure 1. In-vitro cell binding assay. ^{131}I-IgG and ^{131}I-Atezolizumab cell binding experiments in different cell lines (Hela, A375, H460, RKO, and HCT8). RKO cells and ^{131}I-Atezolizumab had the highest binding capacity.
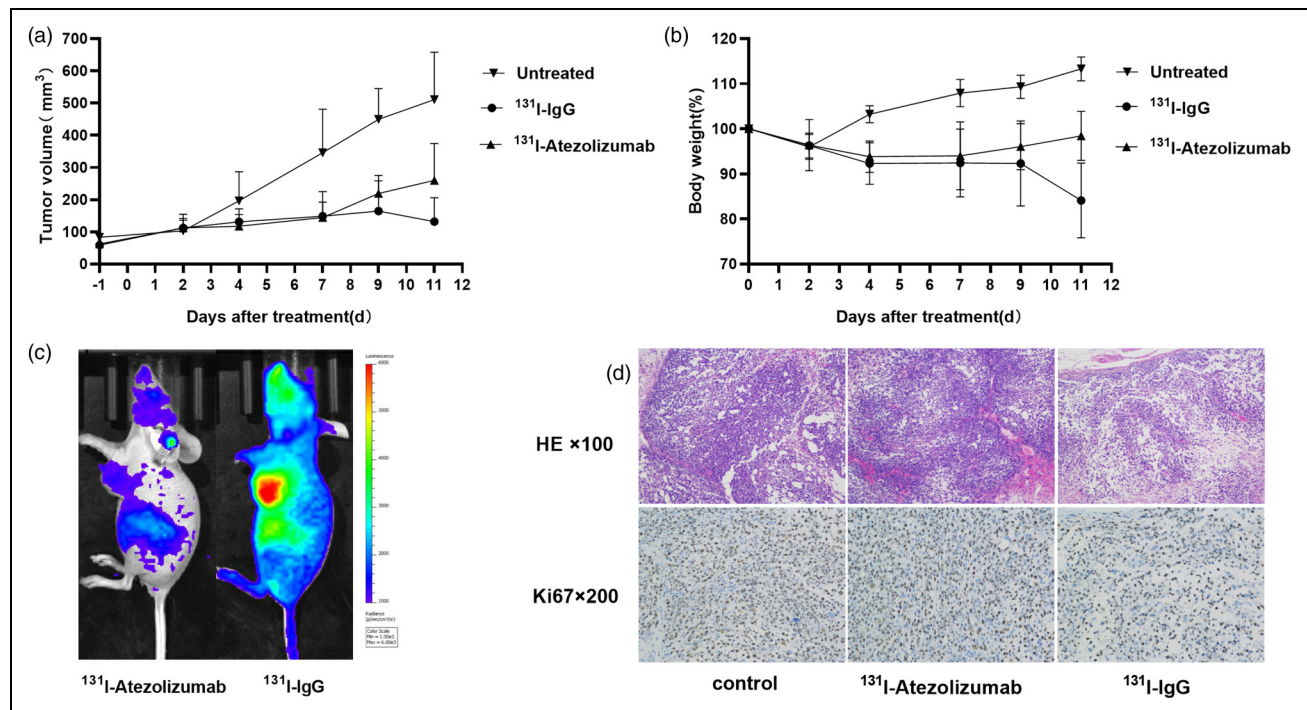

Figure 2. ^{131}I-Atezolizumab and ^{131}I-IgG treatment effect evaluation. (a) Tumor volume change. (b) Mouse body weight changes. (c) CLI of mice 11 days after administration. (d) HE staining and Ki-67 immunohistochemical chemistry.

that before treatment, while no significant weight loss was found in the ^{131}I-Atezolizumab treatment group.

HE Staining and Immunohistochemistry Analysis

After 12 days of treatment, all mice were euthanized, and the proliferation of RKO xenografts was evaluated by Ki-67 staining (Figure 2d). Ki-67 staining in ^{131}I-IgG group was significantly lower than that in untreated group and ^{131}I-Atezolizumab

treatment group. HE staining demonstrated that the tumor showed more divergent necrotic areas in the untreated group and ^{131}I-Atezolizumab treatment group, while the tumor necrosis range was significantly increased in ^{131}I-IgG group.

IR-Atezolizumab and IR-IgG NIRF Imaging

In the RKO model, tumor tracer uptake (TTU) was different in different mice at 24 and 72 h after injection of

IR-Atezolizumab or IR-IgG. The tracer uptake was significantly reduced in the tumor of mice injected with IR-Atezolizumab at 168 h, but there were still many tracers in the tumor of mice injected with IR-IgG (Figure 3). This finding was similar to the results of CLI on the 11th day of administration. In addition, we observed tracer uptake in the pharyngeal lymphatic ring of mice injected with IR-Atezolizumab at 24 and 72 h, but not in mice injected with IR-IgG (Figure 3). This may indicate that lymphoid tissue can also bind to IR-Atezolizumab.

^{131}I-IgG CLI in the 5 Models

^{131}I-IgG CLI technique was used to study the behavior of IgG in 5 tumor models (Hela, A375, H460, RKO, and HCT8). Figure 4a shows representative ^{131}I-IgG CLI of changes over time. Most tumors were clearly visible at 24 h and increased relative fluorescence intensity over time, reaching 1.5 to 2.7 times of muscle fluorescence intensity at 120 h (Figure 4b). In another study, we re-established HCT8 subcutaneous tumor model. After intravenous injection of ^{131}I-Atezolizumab, we found that the tumor was unclear at any time point, and the fluorescence signal intensity of the tumor at 120 h was 1.3 times that of the muscle (Figure 4b). The relative fluorescence intensity of HCT8 tumor-bearing mice injected with ^{131}I-Atezolizumab at various time points (24-120 h) was significantly lower than that injected with ^{131}I-IgG in the first study ($P <$ .001, .002, .003, .012, .002). In addition, we also monitored the tumor growth of mice before and after imaging in the 2 studies (Figure 4c). We found that the growth rates of the tumors were relatively fast in all of these models. Among the mouse models injected with ^{131}I-IgG, Hela mice had the slowest growth rate and the worst visual assessment of IgG imaging. We suspect that the growth rate of tumors may be related to the non-specific uptake of tumors, but more rigorous experiments are needed to verify it.

NIRF/CL Dual-Modality In-situ Imaging In-vivo

Due to the different imaging methods of NIRF imaging and CLI, the imaging ability of the 2 cannot be simply and roughly compared by the average fluorescence intensity or the relative fluorescence intensity. However, we can see the trend of tumor fluorescence intensity changing with time. After the RKO and HCT8 tumor-bearing mice were injected with the mixture of IR-Atezolizumab and ^{131}I-IgG, both NIRF imaging and CLI showed high fluorescence signal intensity in the tumor, and gradually decreased with time (Figure 5). Compared with NIRF imaging, the decline in fluorescence signal of CLI was significantly slower and became more pronounced at later time points.

NIRF/CL Dual-Modality In-situ Distribution Imaging Studies

We noted that RKO and HCT8 tumor tissues had the highest average fluorescence intensity on IR-Atezolizumab NIRF distribution imaging, which could reach (3.24 ± 0.09) and (2.07 ± 0.38) times of muscle, respectively (Figure 6a, b, e and f). The relative fluorescence intensity of RKO tumors was higher than that of HCT8 tumors, which was consistent with the level of PD-L1 expression on the tumor cell surface.

RKO and HCT8 tumors also had the highest average fluorescence intensity on ^{131}I-IgG CLI, which could reach (4.67 ± 1.13) and (4.34 ± 0.5) times of muscle, respectively (Figure 6c, d, g and h). In addition, the blood also had high fluorescence intensity, which were (1.87 ± 0.37) times and (2.04 ± 0.14) times that of muscle, respectively.

Ex-vivo Biodistribution of ^{131}I-Atezolizumab and ^{131}I-IgG

At 24, 72, and 168 h after ^{131}I-Atezolizumab injection, TTU of RKO model was (6.23 ± 0.96), (6.09 ± 1.29), (2.18 ± 1.44) %ID/g, respectively. TTU of HCT8 model was (5.63 ± 0.82), (4.61 ± 1.25), (1.00 ± 0.31) %ID/g, respectively.

At 24, 72, and 168 h after ^{131}I-IgG injection, TTU of RKO model was (10.17 ± 4.62), (13.41 ± 3.69), (8.5 ± 6.4) %ID/g, respectively. TTU of HCT8 model was (11.55 ± 2.83), (7.62 ± 1.51), (8.7 ± 3.36) %ID/g, respectively. The uptake of tumor injected with ^{131}I-IgG at any time point was higher than that of tumor injected with ^{131}I-Atezolizumab. In addition, blood and spleen also have higher uptake (Figure 7a-c).

Discussion

Antibodies are a class of immunoglobulins that can specifically bind to antigens. They can provide extremely high binding affinity and specificity to their target antigen. Therefore, non-invasive imaging with labeled antibodies is an excellent choice for detecting the expression of target antigens in tumors.[22–24] In order to detect the expression level of tumor target antigens in vivo, it is usually necessary to control with non-specific isotype-matched antibodies.[25–28] We found that the optical visualization ability of radionuclide ^{131}I or NIRF dyes labeled IgG in tumors was significantly better than that of radionuclide ^{131}I or NIRF dyes labeled Atezolizumab in the PD-L1-expressing RKO and HCT8 tumor-bearing nude mouse models. ^{131}I-IgG (33.3 MBq) could retain high radioactivity in 5 tumor models (Hela, H460, A375, RKO, HCT8) for a long time and even reduce the size of RKO tumors.

It is doubtful that ^{131}I-IgG can be concentrated in small RKO tumors for a long time and produce anti-tumor effect. The most likely reason is that ^{131}I-IgG can be imaged and treated is a significant enhanced permeability and retention
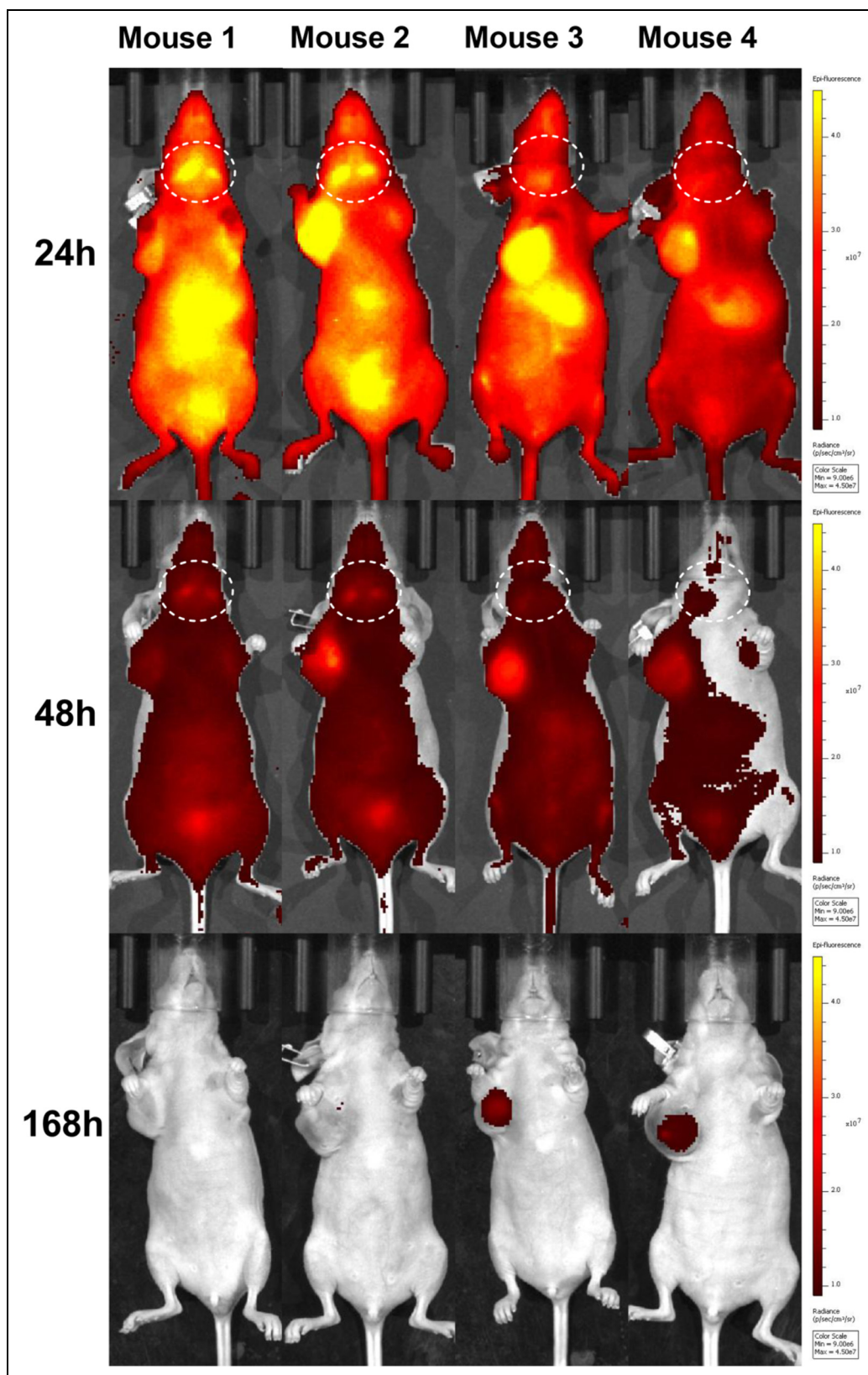
Figure 3. IR-Atezolizumab and IR-IgG NIRF imaging in RKO model. IR-Atezolizumab was injected into mouse 1 and 2, IR-IgG was injected into mouse 3 and 4. Mouse 1 and 2 had no tracer uptake, while mouse 3 and 4 had significant tracer uptake in the pharyngeal lymphatic ring (dotted line).
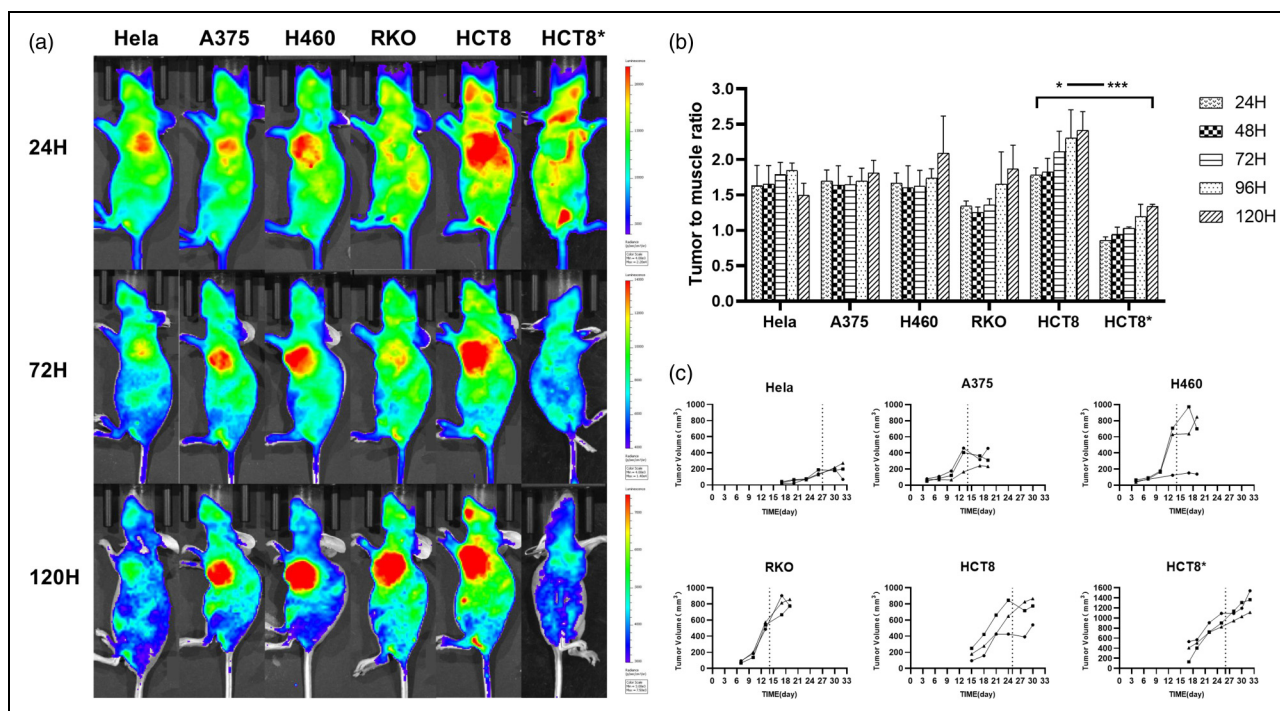
Figure 4. CLI in different mouse models. (a)[131]I-IgG CLI in different mouse models (Hela, A375, H460, RKO, and HCT8 models);[131]I-Atezolizumab CLI in HCT8* model. (b) The relative fluorescence intensity (tumor-to-muscle uptake ratio) of ^{131}I-IgG or ^{131}I-Atezolizumab in different mouse models within 1 to 5 days (n = 3/group). (c) Growth curves of tumors of different models (n = 3/group). Hela, A375, H460, RKO,HCT8 model injected with ^{131}I-IgG, HCT8* model injected with ^{131}I-Atezolizumab, and the dotted line represents the time of drug injection.

effect (ERP effect). Macromolecules with long circulation times (eg, liposomes, nanoparticles, antibodies) are more likely to infiltrate tumor tissue, where they remain for a long time due to blocked lymphatic drainage, so this process is known as the EPR effect. Due to the prevalence of the EPR effect, many researchers are currently working on the preparation of drugs that enhance the ERP effect for non-specific imaging and treatment of tumors.[29–31] The size of the IgG molecule is larger than the renal clearance threshold, so it is not easily cleared by the kidneys quickly. [131]I has a long half-life and can circulate in vivo for a longer time after being coupled with macromolecules IgG, which significantly increases the chance of extravasation. In order to determine whether ^{131}I-IgG imaging ability of RKO tumor is related to tumor type, we performed ^{131}I-IgG CLI in subcutaneous tumor-bearing models of human cervical cancer (Hela), malignant melanoma (A375), large cell lung cancer (H460), and colorectal cancer (RKO, HCT8). Most models had clear images at 24 h, and the relative fluorescence intensity of the tumor increased gradually with time. In addition, we noticed a common feature of these 5 models, namely, faster tumor growth, which may be one of the reasons for the apparent accumulation of radionuclides in the tumors. Bolkestein[32] used radioactive ^{111}In-labeled liposomes to evaluate the

influencing factors of EPR effect in 9 tumor models. He found that tumor vascular density, lymphatic density, hypoxia, and infiltrating macrophages were not the key factors affecting ERP effect. Non-specific imaging was significantly associated with tumor growth. Rapidly growing tumors showed higher tracer uptake. From the growth curves (Figure 4c) of the 5 models, we found that the growth rate of our model mice was faster than that of Bolkestein's study, which may lead to enhanced EPR effects. Furthermore, Niu[33] found that ^{90}Y-labeled nonspecific IgG could passively aggregate in UM-SCC-22B tumors for tumor visualization and treatment due to the high vascular permeability of tumor vessels. Finally, the faster growth rate of the tumor inevitably led to necrosis of the tumor, and we could see scattered multiple foci of necrosis within the tumor on the 17 day HE staining of the tumor transplantation. Studies had shown that the distribution of nonspecific tracer uptake in tumors is concentrated in the necrotic zone.[17,34] ^{131}I-IgG which is concentrated in the necrotic area, has a long half-life. It can emit beta and gamma rays that deliver radiation to surrounding cancer cells, and beta rays can induce cytotoxic effects to promote ultimately cancer cell death. Therefore, it is possible that therapeutic radionuclide labeled nonspecific IgG can visualize tumors and inhibit tumor growth.
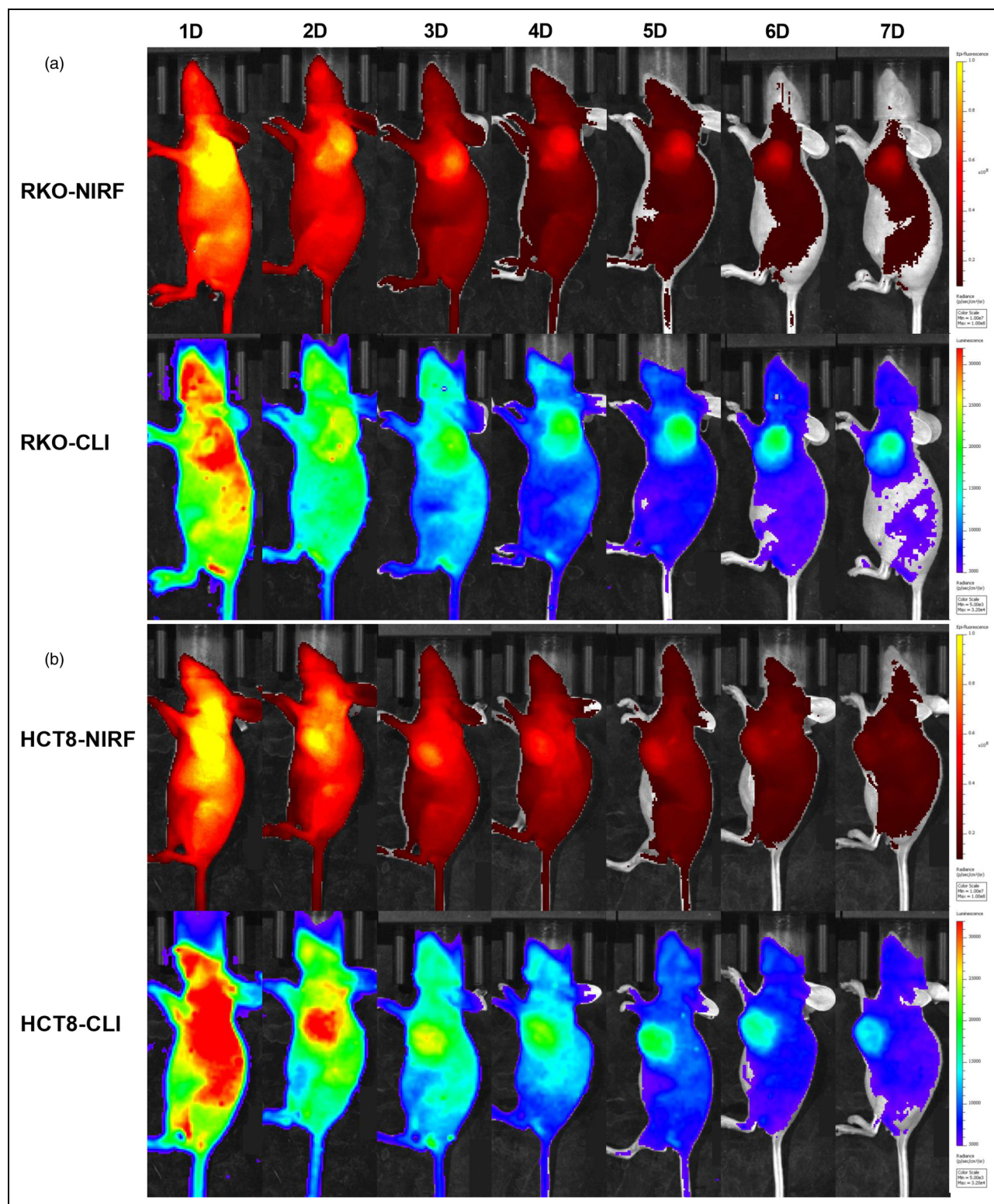
Figure 5. NIRF/CL dual-modality in-situ imaging. (a) NIRF/CL in-situ imaging in RKO mouse model. (b) NIRF/CL in-situ imaging in HCT8 mouse model.
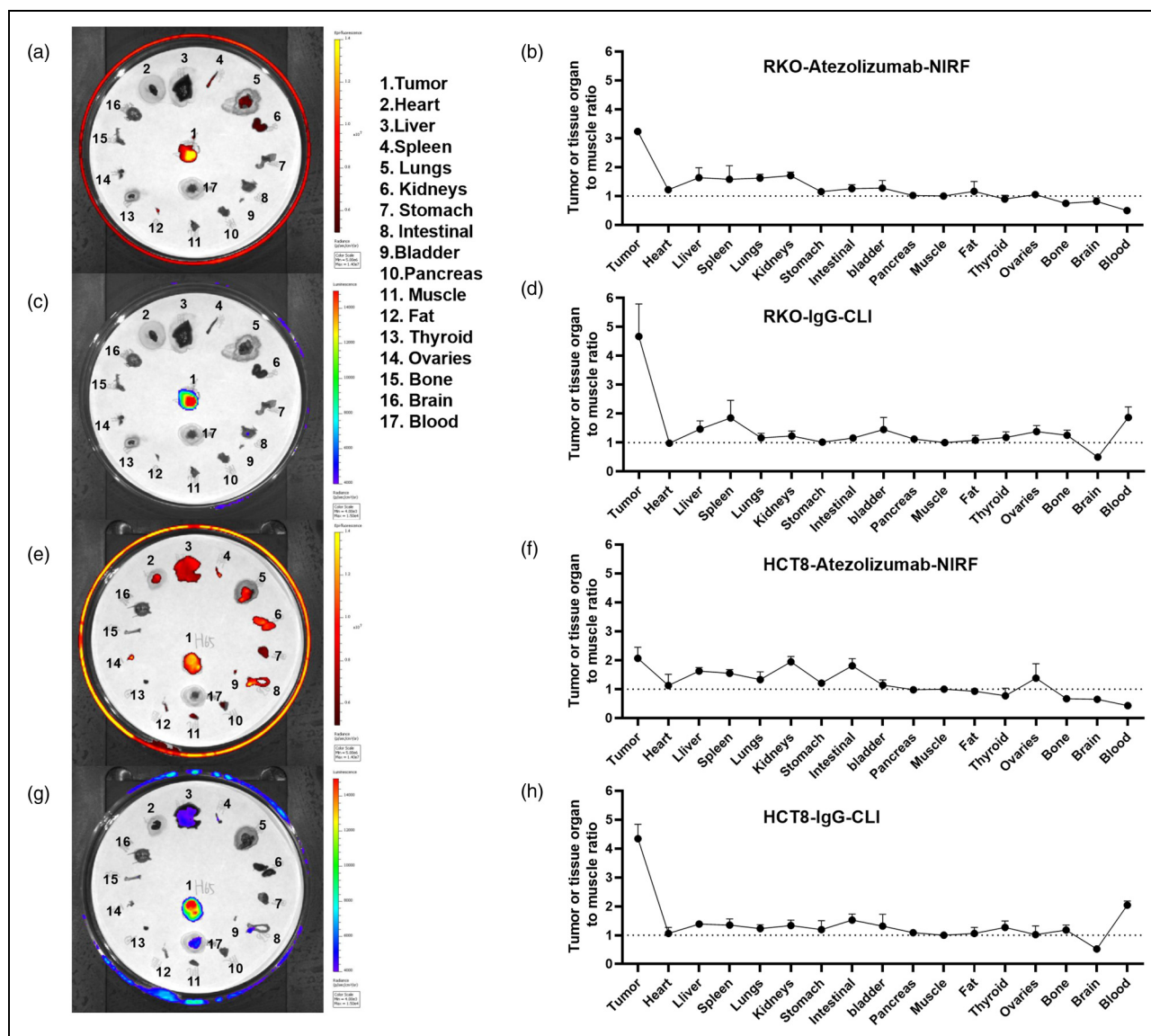
Figure 6. NIRF/CL in-situ distribution imaging at 168 h after administration. (a and b) IR-Atezolizumab NIRF imaging in RKO model. (c and d) ^{131}I-IgG CLI in RKO model. (e and f) IR-Atezolizumab NIRF imaging in HCT8 model. (g and h) ^{131}I-IgG CLI in HCT8 model. The dotted line is the mean fluorescence intensity of the muscle.

Atezolizumab is a humanized monoclonal IgG1 targeting PD-L1 with a molecular weight of 145 kDa. The control IgG is a human lgG1 isotype control antibody with a molecular weight of 150 kDa and no binding ability to tumor cells. The 2 antibodies are monoclonal IgG1 with similar molecular weights, and their binding methods with radionuclides or NIRF are similar. Why is the ability of tumor non-specific imaging better than specific imaging? From the early stage of IR-Atezolizumab and IR-IgG NIRF imaging, we can see that there were different TTU, and there was heterogeneity in tumor uptake between the same group and different groups. Because optical imaging is susceptible to tissue depth and the uptake of tumor tracers is heterogeneous, the influence of body position on imaging is substantial. Other

molecular imaging devices, such as microPET and SPECT, can overcome these problems. However, their widespread use is limited due to the high cost, the need for special instruments, and the long time for data collection. On the contrary, optical imaging has become an important tool for small animal imaging because of its high sensitivity, fast imaging speed, ability to image multiple animals at the same time, low price, and easy operation. NIRF/CLI dual-modality in-situ imaging can achieve completely consistent position, which greatly eliminates the influence of individual mouse differences, internal environment differences and mouse body position on the imaging. At the same time, the experimental animals are reduced by half. Due to the different labeling methods of IR-Atezolizumab and ^{131}I-IgG, the
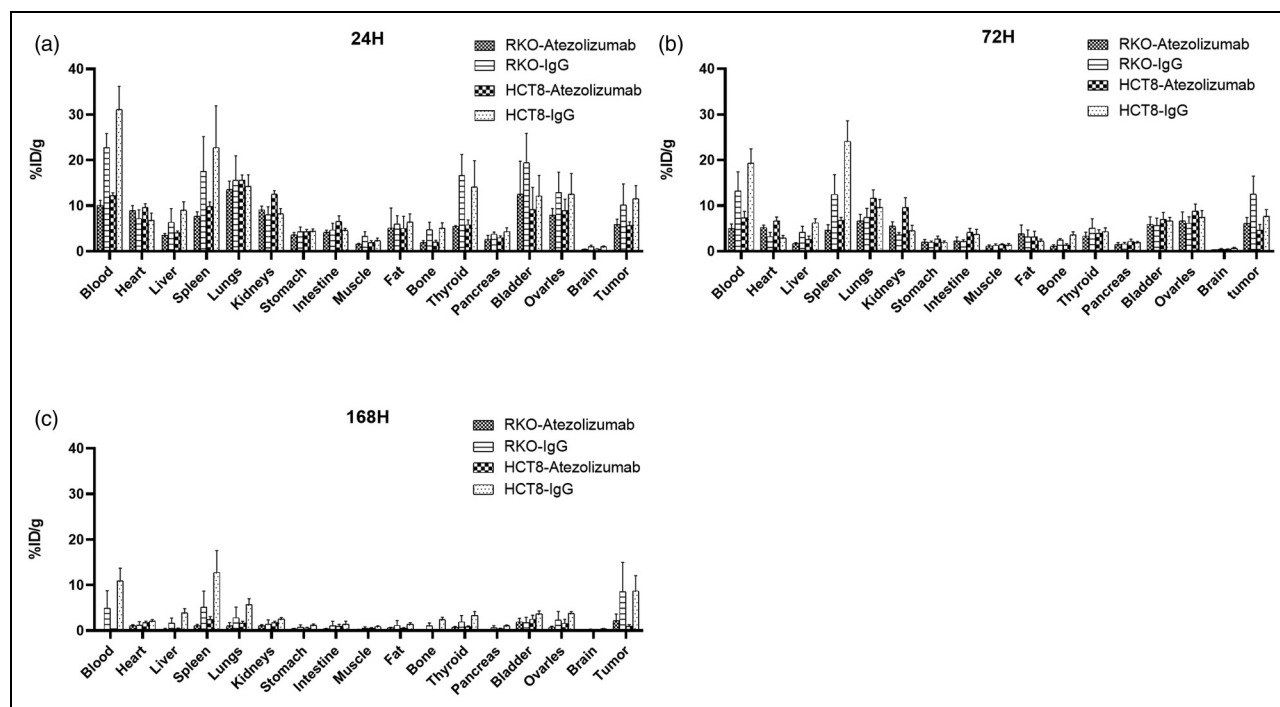
Figure 7. In-vitro tissue distribution at different time points. (a, b and c) Distribution of tumor and organs in mice at 24, 72, 168 h after administration.

same protein amount cannot be labeled. In order to ensure the same metabolism in-vivo, 53 μg non-radioactive IgG was added into the mixture. We found similar results for the mouse homozygous and heterozygous controls.

Distinct from other experiments,[35] our experiments were performed using immunodeficient mice, which lack mature T cells, so tumor-infiltrating T cells are deficient, which inevitably leads to a decrease in the amount of PD-L1-expressing cells within the tumor. Nude mice were treated with ^{131}I-Atezolizumab, which mainly uses the specific immune binding of Atezolizumab and PD-L1. Thus, it does not elicit subsequent immune responses. Studies have shown that Atezolizumab can cross-react with mouse PD-L1.[12,36] Labeled Atezolizumab can not only bind to tumor cells, but also to other tissues, organs, or immune cells expressing PD-L1. Due to the widespread expression of PD-L1, the chance of specific uptake and passive extravasation of the tracer is reduced. However, IgG does not bind to tumor cells, nor to other tissues and organs expressing PD-L1, which significantly increases the chances of extravasation of imaging agents in tumors and makes more imaging agents accumulate in tumor tissues. In a study, Ehlerdin[26] injected [89]Zr-Df-IgG into nude mice carrying A549 tumor cells and performed PET imaging. The uptake of [89]Zr-Df-IgG in tumor reached a peak at 72 h and then decreased slowly, reaching (4.4 ± 1.3) %ID/g at 120 h. In another study of [89]Zr-Df-Atezolizumab PET imaging, Ehlerdin[37] found that the uptake value of A549 tumor without PD-L1 expression reached the peak at 12 h, which

was (2.38 ± 0.67) % ID/g, and that of H460 tumor with PD-L1 expression reached the peak at 24 h, which was only (2.10 ± 0.52) %ID/g. The uptake of [89]Zr-Df-tezolizumab in tumors at any time point was significantly lower than the uptake of [89]Zr-Df-IgG in previous studies. He also found clear lymphatic networks in nude mice injected with [89]Zr-Df-Atezolizumab. In our IR-Atezolizumab NIRF imaging study, we can see obvious and persistent tracer uptake in the pharyngeal lymphatic ring, but not in mice injected with IR-IgG. It also shows that Atezolizumab can bind to the lymphatic tissue of mice (Figure 3). In addition, Moroz[36] found that TTU was lower in nude mice injected with high specific activity [89]Zr-Df-Atezolizumab (2.5 μCi/μg), while injected with low specific activity [89]Zr-Df-Atezolizumab (0.16 μCi/μg), the uptake of tracers in normal tissues was blocked and the TTU was significantly increased. Thus, the uptake of tracer by normal tissue expressing PD-L1 would significantly affect the uptake of tracer by tumor. Since the original purpose of our experiments was to explore radioimmuno-therapy with ^{131}I-Atezolizumab, the specific activities of the drugs used for both ^{131}I-Atezolizumab and ^{131}I-IgG imaging and treatment were relatively high (12.8-47.37 μCi/μg). Therefore, it is possible that tumor specific imaging of ^{131}I or NIR dyes labeled Atezolizumab is not as good as that of non-specific IgG imaging.

So far, we have not yet fully explained the abnormal biological distribution of ^{131}I-IgG in the spleen in-vitro distribution experiments, which may be related to Fc receptor

involvement. Sharma[38] found that much of the anomalous biodistribution of humanized antibody drugs in immunodeficient mice may be attributed to an avid Fc-mediated binding of these agents to FcR-expressing myeloid cells in non-target organs when endogenous immunoglobulin levels are low or nearly absent. We also do not know whether there are other mechanisms involved in the result that IgG imaging is superior to Atezolizumab imaging. It is still unclear whether other non-specific IgG will appear similar to our results. Notably, a large number of studies have shown that EPR effects play a role in rodents but not in humans.[39] Therefore, this result may not appear in the human body.

Conclusions

Molecular imaging technology often uses radionuclides or fluorescent dyes to label monoclonal antibodies to study the expression level of cancer-related antigens in malignant tumors. In the selection of control, we should consider the influence of the range and degree of antigen expression in tissues and organs, the physical and chemical properties of macromolecular drugs and the EPR effect on tumor imaging, etc. Sometimes these influences are great and may eventually lead to wrong conclusions.

In summary, non-specific IgG may not be suitable as a negative control to compare the expression level of PD-L1 in optical imaging of radionuclide ^{131}I or NIR dyes labeled Atezolizumab in a human-derived tumor nude mouse model under certain circumstances.

Abbreviations

anti-PD-1/PD-L1	anti-programmed cell death-1/programmed cell death-Ligand 1
BSA	bovine serum albumin
CL	Cerenkov luminescence
CLI	Cerenkov luminescence imaging
ERP	effect enhanced permeability and retention effect
FBS	fetal bovine serum
FDA	the U.S. Food and Drug Administration
131I-Atezolizumab	^{131}I-labeled Atezolizumab
131I-IgG	^{131}I-labeled human non-specific IgG1
IR-Atezolizumab	IRDye®800 CW labeled Atezolizumab
IR-IgG	IRDye®800 CW labeled IgG
NIRF	near-infrared fluorescence
NIRF/CL	near-infrared fluorescence/Cerenkov luminescence
PB	phosphate buffer
PBS	phosphate buffer saline
PD-L1	programmed cell death-Ligand 1
TTU	tumor tracer uptake

Author Contributions

Linhan Zhang, Lianmeng Zhao, Xue Lin, Sheng Zhao, Wenbin Pan, Zhongqi Sun, Dandan Wang, Jinping Li contributed to conceptualization, investigation, visualization, formal analysis and writing original draft. Rongjun Zhang contributed to conceptualization, methodology, writing review and editing. Huijie Jiang and Zonghui Liang contributed to conceptualization, resources, supervision, project administration, funding acquisition. All authors critically revised and edited the manuscript and approved the final draft.

Availability of Data and Materials

All data generated or analyzed during this study are included in this published article.

Declaration of Conflicting Interests

The authors declared no potential conflicts of interest with respect to the research, authorship, and/or publication of this article.

Funding

Statement of Ethical Declaration

All procedures were performed with the approval of the Institutional Animal Care and Use Committees of Jiangsu Institute of Nuclear Medicine. All methods were carried out in accordance with relevant guidelines and regulations. The study was carried out in compliance with the ARRIVE guidelines.

ORCID iD

Huijie Jiang ⓘD https://orcid.org/0000-0001-7321-5297

References

1. Herbst RS, Soria J-C, Kowanetz M, et al. Predictive correlates of response to the anti-PD-L1 antibody MPDL3280A in cancer patients. *Nature*. 2014;515(7528):563-567.

2. Meng X, Huang Z, Teng F, et al. Predictive biomarkers in PD-1/PD-L1 checkpoint blockade immunotherapy. *Cancer Treatment Rev*. 2015;41(10):868-876.

3. Wan H, Ma H, Zhu S, et al. Developing a bright NIR-II fluorophore with fast renal excretion and its application in molecular imaging of immune checkpoint PD-L1. *Adv Funct Mater*. 2018; 28(50):1804956.

4. Qin S, Yu Y, Guan H, et al. A preclinical study correlation between PD-L1 PET imaging and the prediction of therapy. *Aging (Albany NY)*. 2021;13(9):13006-13022.

5. Mishra A, Gupta K, Kumar D, et al. Non-invasive PD-L1 quantification using [18F]DK222-PET imaging in cancer immunotherapy. *J ImmunoTherapy Cancer*. 2023;11(10):e007535.

6. Sharma G, Braga MC, Da Pieve C, et al. Immuno-PET imaging of tumour PD-L1 expression in glioblastoma. *Cancers (Basel)*. 2023;15(12):3131.

7. Akinboro O, Larkins E, Pai-Scherf LH, et al. FDA Approval Summary: Pembrolizumab, Atezolizumab, and Cemiplimab-rwlc as single agents for first-line treatment of advanced/metastatic PD-L1–high NSCLC. *Clin Cancer Res*. 2022;28(11):2221-2228.

8. Casak SJ, Donoghue M, Fashoyin-Aje L, et al. FDA Approval Summary: Atezolizumab plus Bevacizumab for the treatment of patients with advanced unresectable or metastatic hepatocellular carcinoma. *Clin Cancer Res*. 2021;27(7):1836-1841.

9. Mathieu LN, Larkins E, Sinha AK, et al. FDA Approval Summary: Atezolizumab as adjuvant treatment following surgical resection and platinum-based chemotherapy for stage II to IIIA NSCLC. *Clin Cancer Res*. 2023;29(16):2973-2978.

10. Bensch F, Van Der Veen EL, Lub-De Hooge MN, et al. 89Zr-Atezolizumab Imaging as a non-invasive approach to assess clinical response to PD-L1 blockade in cancer. *Nature Med*. 2018;24(12):1852-1858.

11. Lesniak WG, Chatterjee S, Gabrielson M, et al. PD-L1 detection in tumors using [64Cu]Atezolizumab with PET. *Bioconjugate Chem*. 2016;27(9):2103-2110.

12. Chatterjee S, Lesniak WG, Gabrielson M, et al. A humanized antibody for imaging immune checkpoint ligand PD-L1 expression in tumors. *Oncotarget*. 2016;7(9):10215-10227.

13. Vento J, Mulgaonkar A, Woolford L, et al. PD-L1 detection using (89)Zr-Atezolizumab immuno-PET in renal cell carcinoma tumorgrafts from a patient with favorable Nivolumab response. *J Immunother Cancer*. 2019;7(1):144.

14. Massicano AVF, Song PN, Mansur A, et al. [89Zr]-Atezolizumab-PET Imaging reveals longitudinal alterations in PDL1 during therapy in TNBC preclinical models. *Cancers (Basel)*. 2023;15(10):2708.

15. Zhao S, Pan W, Jiang H, et al. Cerenkov luminescence imaging is an effective preclinical tool for assessing colorectal cancer PD-L1 levels in vivo. *EJNMMI Res*. 2020;10(1):64.

16. Zhang L, Zhao S, Jiang H, et al. Radioimmunotherapy study of (131)I-labeled Atezolizumab in preclinical models of colorectal cancer. *EJNMMI Res*. 2022;12(1):70.

17. Knight JC, Mosley MJ, Kersemans V, et al. Dual-isotope imaging allows in vivo immunohistochemistry using radiolabelled antibodies in tumours. *Nuclear Med Biol*. 2019;70:14-22. doi:10.1016/j.nucmedbio.2019.01.010.

18. Grootendorst MR, Cariati M, Kothari A, et al. Cerenkov luminescence imaging (CLI) for image-guided cancer surgery. *Clin Transl Imaging*. 2016;4(5):353-366.

19. Lee HJ, Ehlerding EB, Jiang D, et al. Dual-labeled pertuzumab for multimodality image-guided ovarian tumor resection. *Am J Cancer Res*. 2019;9(7):1454-1468.

20. Li M, Wei W, Barnhart TE, et al. ImmunoPET/NIRF/Cerenkov multimodality imaging of ICAM-1 in pancreatic ductal adenocarcinoma. *Eur J Nucl Med Mol Imaging*. 2021;48(9):2737-2748.

21. Aherne GW, James SL, Marks V. The radioiodination of bleomycin using iodogen. *Clin Chim Acta*. 1982;119(3):341-343.

22. Cavaliere A, Sun S, Lee S, et al. Development of [(89)Zr]ZrDFO-amivantamab bispecific to EGFR and c-MET for PET imaging of triple-negative breast cancer. *Eur J Nucl Med Mol Imaging*. 2021;48(2):383-394.

23. Facca VJ, Al-Saden N, Ku A, et al. Imaging of HER2-positive tumors in NOD/SCID mice with pertuzumab fab-hexahistidine peptide immunoconjugates labeled with [(99m)Tc]-(I)-tricarbonyl complex. *Mol Imaging Biol*. 2021;23(4):495-504.

24. Lu Y, Li M, Massicano AVF, et al. (89Zr]-pertuzumab PET imaging reveals paclitaxel treatment efficacy is positively correlated with HER2 expression in human breast cancer xenograft mouse models. *Molecules*. 2021;26(6):1568.

25. Chang YJ, Ho CL, Cheng KH, et al. Biodistribution, pharmacokinetics and radioimmunotherapy of (188)Re-cetuximab in NCI-H292 human lung tumor-bearing nude mice. *Invest New Drugs*. 2019;37(5):961-972.

26. Ehlerding EB, England CG, Jiang D, et al. CD38 as a PET imaging target in lung cancer. *Mol Pharm*. 2017;14(7):2400-2406.

27. Wei W, Jiang D, Rosenkrans ZT, et al. HER2-targeted multimodal imaging of anaplastic thyroid cancer. *Am J Cancer Res*. 2019;9(11):2413-2427.

28. Kang L, Jiang D, England CG, et al. ImmunoPET imaging of CD38 in murine lymphoma models using (89)Zr-labeled daratumumab. *Eur J Nucl Med Mol Imaging*. 2018;45(8):1372-1381.

29. Gong Z, Zhou B, Liu X, et al. Enzyme-induced transformable peptide nanocarriers with enhanced drug permeability and retention to improve tumor nanotherapy efficacy. *ACS Appl Mater Interfaces*. 2021;13(47):55913-55927.

30. Wu H, Li W, Hao M, et al. An EPR-Independent extravasation strategy: Deformable leukocytes as vehicles for improved solid tumor therapy. *Adv Drug Deliv Rev*. 2022;187:114380. doi:10.1016/j.addr.2022.114380.

31. Kim J, Cho H, Lim D-K, et al. Perspectives for improving the tumor targeting of nanomedicine via the EPR effect in clinical tumors. *Int J Mol Sci*. 2023;24(12):10082.

32. Bolkestein M, De Blois E, Koelewijn SJ, et al. Investigation of factors determining the enhanced permeability and retention effect in subcutaneous xenografts. *J Nucl Med*. 2016;57(4):601-607.

33. Niu G, Sun X, Cao Q, et al. Cetuximab-based immunotherapy and radioimmunotherapy of head and neck squamous cell carcinoma. *Clin Cancer Res*. 2010;16(7):2095-2105.

34. Heneweer C, Holland JP, Divilov V, et al. Magnitude of enhanced permeability and retention effect in tumors with different phenotypes: 89zr-albumin as a model system. *J Nucl Med*. 2011;52(4):625-633.

35. Wen X, Zeng X, Liu J, et al. Synergism of 64Cu-labeled RGD with anti-PD-L1 immunotherapy for the long-acting antitumor effect. *Bioconjugate Chem*. 2022;33(11):2170-2179.

36. Moroz A, Lee C-Y, Wang Y-H, et al. A preclinical assessment of 89Zr-Atezolizumab identifies a requirement for carrier added formulations not observed with 89Zr-C4. *Bioconjugate Chem*. 2018;29(10):3476-3482.

37. Ehlerding EB, Lee HJ, Barnhart TE, et al. Noninvasive imaging and quantification of radiotherapy-induced PD-L1 upregulation with 89Zr-Df–Atezolizumab. *Bioconjugate Chem*. 2019;30(5):1434-1441.

38. Sharma SK, Chow A, Monette S, et al. Fc-mediated anomalous biodistribution of therapeutic antibodies in immunodeficient mouse models. *Cancer Res*. 2018;78(7):1820-1832.

39. Danhier F. To exploit the tumor microenvironment: Since the ERP effect fails in the clinic, what is the future of nanomedicine?. *J Control Release*. 2016;244(Pt A):108-121.